

Article

An Experimental Study on Deuterium Production from Titanium Hydride Powders Subjected to Thermal Cycles

Luca Gamberale ^{1,2,3} and Giovanni Modanese ^{4,*} ¹ Quantumatter Inc., 277 West End Ave. #7D, New York, NY 10023, USA; luca.gamberale@unimib.it² Leda Srl, Corso Monforte 19, 20122 Milano, Italy³ Physics Department, University of Milano-Bicocca, Piazza della Scienza 3, 20126 Milano, Italy⁴ Faculty of Engineering, Free University of Bozen-Bolzano, 39100 Bolzano, Italy

* Correspondence: giovanni.modanese@unibz.it

Abstract: An extensive multi-year experimental study was conducted to investigate the potential production of deuterium from titanium hydride TiH_x powders subjected to specific thermal cycles. Mass spectrometry was performed, focusing on the variation in signal intensities at $m/z = 2, 3, 4, 18, 19, 20,$ and 21 , corresponding to fragments primarily involving deuterium, during the degassing of titanium hydride powders as the sample temperature was raised from room temperature to approximately $1100\text{ }^\circ\text{C}$. The results reveal an anomaly in the deuterium-to-hydrogen ratios, with the analysis indicating an increase in deuterium concentration by a factor of approximately 280 compared to its natural concentration on Earth. Three independent methods confirmed the excess deuterium. Simultaneously, flow calorimetry was performed during the degassing process, which did not show any measurable excess heat produced in the configuration used. This study was motivated by our novel theoretical predictions, based on the standard electroweak theory with gauge symmetry, suggesting the generation of slow neutrons within metal hydrides when exposed to coherent excitations. Our findings align with direct measurements of neutron emission by TiH_x powders under cavitation in liquid water, as recently published by Fomitchev-Zamilov.

Keywords: deuterium production; titanium hydride; thermal cycles; slow neutrons; metal hydrides



Citation: Gamberale, L.; Modanese, G. An Experimental Study on Deuterium Production from Titanium Hydride Powders Subjected to Thermal Cycles. *Symmetry* **2024**, *16*, 1542. <https://doi.org/10.3390/sym16111542>

Academic Editor: Christophe Humbert

Received: 13 September 2024

Revised: 27 October 2024

Accepted: 12 November 2024

Published: 18 November 2024



Copyright: © 2024 by the authors. Licensee MDPI, Basel, Switzerland. This article is an open access article distributed under the terms and conditions of the Creative Commons Attribution (CC BY) license (<https://creativecommons.org/licenses/by/4.0/>).

1. Introduction

The transmutation of elements at low temperatures has been a subject of intense study for more than thirty years. In this work we describe new experimental evidence of the production of deuterium from titanium powder loaded with hydrogen. We will also discuss the theoretical hypothesis that this deuterium is produced by a reaction in which protons in an excited coherent state generate slow neutrons via electronic capture; it naturally follows that these neutrons are also able to cause a wide range of nuclear transmutations involving heavy elements. In the first part of this introduction we are thus going to recall the main experimental evidence of transmutations occurring in various low-energy conditions, as we believe that their explanation is strictly related to the hypothesized coherent neutron generation.

Evidence of the emission of neutrons from a titanium–deuterium system was reported as early as in 1989 by De Ninno et al. [1]. Reports by Ohmori, Mizuno, and co-workers in 1997–1998 [2,3] described the formation of Fe from an Au electrode during electrolysis. In the 2000s, Iwamura et al. [4–6] further advanced the field by demonstrating the generation of Ru and Pr following the permeation of D_2 gas through a Pd membrane. Around the same period, Celani et al. [7,8] reported the detection of new elements in Th-Hg-Pd-D(H) electrolytic systems. For an extensive review of related studies, see [9].

Later, Iwamura et al. found transmutation phenomena induced by deuterium gas permeation through nanosized Pd multilayers doped with Cs and other elements [10–13].

They observed the transmutation of Cs into Pr by this method at the laboratory of Mitsubishi Heavy Industries Ltd. These results have been independently reproduced [14].

Ref. [15] offers a recent detailed analysis of neutron production in low-energy experiments. The collected experimental evidence supports the hypothesis of a new class of nuclear reactions, prompting recent interest from the US Department of Energy's ARPA-E program, which has launched a new initiative to investigate this phenomenon further. In Ref. [16], Fomitchev-Zamilov reported clear observations of neutron emission during the acoustic cavitation of deuterated titanium powder.

Huang et al. have recently conducted experiments using two reactors made from a concentric multiple-pipe heat exchanger and found that, when water is flowing through a tiny space and heated, it produces peculiar excess heat probably by cavitation and the dynamic implosion of nanobubbles [17]. Possible nuclear transmutation was found by SEM/EDX inspection of ruptured copper pipe samples (C increases 200–500%, O 300–600%, Fe 400%, and new elements P, S, and Ca appear).

Very recently, in a correlated study [18], one of the authors (L.G.) illustrated the theoretical viability of generating neutrons through electron capture (EC) (Figure 1) at room temperature and low energy within a metal sample (e.g., Ni, Ti) heavily loaded with hydrogen. This was accomplished by utilizing the coherence properties of the quantum plasma created by dissolved protons within a metal [19–21]. When suitably excited coherently, this plasma can provide enough de-excitation energy to generate a neutron from one of the protons through electronic capture. These predictions are based on the standard model of electroweak interactions, relying on the fundamental $SU(2)_L \times U(1)$ gauge symmetry.

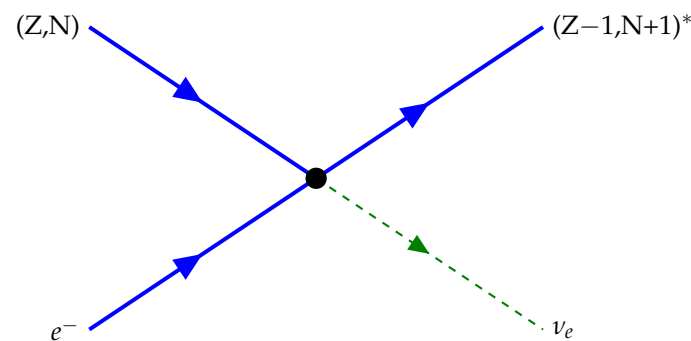


Figure 1. The Feynman diagram depicts the transmutation of a nucleus composed of Z protons and N neutrons into an excited isotope (with symbol $*$) containing $Z - 1$ protons and $N + 1$ neutrons, accompanied by the emission of an electronic neutrino through electron capture. The energy required to initiate this process stems from the coherent vibrational energy inherent in the excited proton plasma.

Previous publications have discussed the production of ultra-slow neutrons in metals [22], but they do not provide a comprehensive treatment of the energy exchange required to overcome the mass gap for neutron production.

The novel underlying principle supporting the theory developed in [19] is that, through a coherent process, the energy required to reach the threshold for neutron production can be supplied by a coherent superposition of energy quanta associated with highly populated low-energy degrees of freedom. These degrees of freedom encompass the vibrational modes of the electron and/or proton plasmas.

Specifically, electron capture becomes possible because the coherent plasmas of protons and electrons present in the metal [19] in particular conditions, when coherently excited to an elevated vibrational state, possess an energy that is significantly higher compared to typical thermal energies. This is because the plasmas are composed of a vast number of particles, resulting in sufficient energy to overcome the mass gap between the combined mass of a proton and an electron and the mass of a neutron, enabling the production of a neutron and an electronic neutrino.

In simple terms, there are two different ways to quantum mechanically describe a set of N identical particles. The first approach utilizes the density matrix formalism, which represents a statistical ensemble of independent particles whose quantum phases are completely uncorrelated. The second approach involves representing the N particles as a coherent system, wherein all particles share the same quantum phase and are described by a single quantum state.

In the first case, when interacting with another field, the conservation of energy in the transition is associated with the energy of a single particle, which is generally a fraction of an eV. In the second case, the energy associated with the coherent quantum state is the sum of the single particle energies and is equal to N times the energy of a single particle. Consequently, in calculating the transition rate, the energy conservation condition to be imposed contains a coherent energy that is N times larger than that of a single particle and can reach values in the order of MeV.

Thus, it becomes possible for a process to generate a neutron and a neutrino from a coherent state of electrons and protons, as the required energy is 782 keV, corresponding to a very small vibrational energy per proton and per electron. This condition would be impossible to achieve in the case of incoherent transitions and is the reason why, in our opinion, it is impossible to describe LENR phenomena through single-particle theories.

In reference [19], we have shown how these coherent proton states can form spontaneously within a metallic matrix. Considering that electrons in the metal are also in coherent configurations, as shown in reference [23], it becomes possible to rigorously write, within the standard model, a coherent transition rate for neutron production.

The formalism of coherent states for particles of spin 1/2 in a state of high density is not frequently used and requires special care. For this reason we will discuss in more detail these theoretical issues in a separate work.

The neutrons produced in this manner, being generated just above the energy threshold, have a very small momentum and their cross-section of interaction with surrounding nuclei is very high, leading to immediate binding through nuclear capture. This forms metastable nuclear states that quickly decay to their ground state, releasing an energy equal to the nuclear binding energy of the incoming neutron. This energy is not emitted in the form of γ rays because the emitted γ during de-excitation is coherently absorbed by the electron plasma in the crystal. The excitation of the coherent electronic state, being shared by a macroscopic number of electrons, can be effectively dissipated as heat through a downconversion process similar to latent heat production in a phase transition.

As this study is experimental in nature, we will delve deeper into a rigorous theoretical description of the processes outlined in a dedicated work aimed at establishing the foundations for a comprehensive theory of nuclear phenomena in condensed matter.

The objective of this experimental study is to validate the possibility of exciting these coherent configurations to an extent that generates measurable quantities of ultra-low momentum (ULM) neutrons. This is achieved by subjecting Ti micropowders loaded with natural hydrogen ($D/H \sim 10^{-4}$) to thermal cycles.

To this end, we have employed a custom-built reactor, two independent vacuum systems, a residual gas analyzer (RGA), and a mass-flow calorimeter. The experimental procedure was repeated seven times over a time span of more than one year. The gas outgassed from the active samples was analyzed and compared to the gas of a reference hydrogen tank.

Mass spectrometry measurements have revealed an excess of deuterium in comparison to the natural background in all the tests performed. Following the theory described in [18], this excess is thought to be a direct consequence of the generation of slow neutrons in the coherent electron capture reactions described above. More details about this process and further expected consequences of the coherent electron capture are given in the next section.

2. Expected Consequences of Neutron Generation in Our Experimental Environment

The presence of ULM neutrons in the metal naturally induces neutron capture processes [24] by the nuclei present in the surrounding environment, typically hydrogen nuclei

and titanium nuclei. The products of the expected reactions will therefore be mainly deuterium nuclei, tritium nuclei, and titanium isotopes, of which the most abundant isotope is ^{48}Ti with 73.7%.

Since the stable isotopes of Ti range from 46 to 50 in mass number, the addition of a neutron will predominantly produce an isotopic abundance shift without producing observable nuclear effects. Only ^{50}Ti with a natural abundance of 5.2% would transmute to ^{51}Ti which is a beta-emitter with a decay time of 5.8 min to ^{51}V which is again stable.

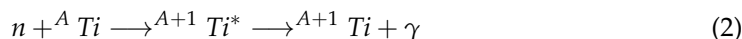
The produced deuterium has the advantage of being released from the metal in gaseous form and is therefore detectable by an RGA after escaping from the metal. The produced tritium would have a much lower abundance than deuterium since it requires the interaction of a neutron with a deuterium nucleus which, being less abundant than hydrogen, implies much suppressed tritium production.

The incoherent (single-particle) process of neutron capture by hydrogen nuclei can be described by the following equation:



where n is a neutron, H is a hydrogen nucleus, D^* is a deuterium nucleus in an excited state, D is a deuterium nucleus in its ground state, and γ is the outgoing photon. The reaction is exothermic, releasing approximately 2.2 MeV of energy. The only available mechanism for energy dissipation is electromagnetic de-excitation, resulting in the emission of a γ photon of approximately 2.2 MeV within a characteristic time given by $\tau \simeq \frac{1}{E} \simeq 2 \cdot 10^{-21}$ s. Consequently, the single-particle process is inherently radioactive.

Likewise, the process of neutron capture by titanium nuclei can be described by the following equation:



where ${}^{A+1}\text{Ti}^*$ is an excited state of titanium. The reaction is also exothermic, releasing an approximately 1.5 MeV photon.

Finally, the production of tritium can be described by the following equation:



where T^* and T are tritium nuclei in the excited and ground states.

In all these cases, the γ rays produced by the de-excitation of the metastable state of the newly formed isotopes denoted by an asterisk, that would normally be radiated away in the vacuum in a timeframe of order $\tau \sim 10^{-6} \text{ eV}^{-1} = 10^{-22}$ s, are not detected outside the host metallic matrix because they are coherently absorbed by the coherent state of electrons present in the metal. The coherent nature of this interaction implies an amplification factor for the electromagnetic coupling constant in the order of $\sqrt{N_e} \sim 10^4$ where N_e is the number of electrons in the coherent state, implying an amplification of the interaction probability of a factor $\sim 10^8$. The γ energy is thus distributed among a large number of electrons, so each acquires a small fraction of an electron volt, which can then be efficiently converted into thermal energy. The result is the absence of γ emissions and an increase in the crystal's temperature due to the conversion of the γ energy into heat.

One might wonder why a metal irradiated by γ rays does not exhibit the same absorption efficiency as observed in the case of photons emitted during the de-excitation of nuclei produced through the previously described mechanism. The reason lies in the fact that, for the reaction to occur, both energy and momentum must be conserved in the interaction with the coherent state of electrons, which effectively makes the phase space nearly zero. In contrast, during the absorption process of the γ photon, since the photon is virtual, energy conservation is not required at the electromagnetic vertex. This results in a much higher interaction rate compared to the first scenario.

In summary, the described reactions primarily generate heat and stable isotopes, with only a minimal fraction of the energy produced in the form of energetic radiation. The produced tritium, due to its radioactivity, should be subsequently observable. How-

ever, the quantity produced is expected to be very small, resulting in negligible levels of radioactivity, as will be further discussed in the following sections. A specialized apparatus should be implemented to detect it.

For completeness, we note that, under certain circumstances, the coherence of the process may not be complete, particularly in situations of strong disequilibrium and impulsive excitation. In these cases, the emission of highly energetic particles can occur, as has been experimentally observed in some setups [25].

Coherent correlated states and low-energy nuclear reactions in nonstationary systems have been analyzed in refs. [26,27].

The authors of [28] investigate possible low energy nuclear reactions arising due to the conversion of proton to neutron through weak interactions, in which the resulting neutron forms a short-lived virtual state, according to the framework of second-order perturbation theory.

3. Methods

The experiment is designed to detect an increase in the concentration of deuterium relative to its natural abundance, which is in the range of $1.5 \cdot 10^{-4}$ – $2.5 \cdot 10^{-4}$, in the gas degassed from a TiH_x sample subjected to thermal cycles ranging from 20 °C to 1100 °C. This measurement is carried out by monitoring the relative heights of signals from an RGA for various hydrogen compounds, typically H_2 , HD , H_2O , and HDO . The following subsections describe the experimental setup and the procedures for conducting the experiments.

3.1. Experimental Setup

The experimental apparatus (Figure 2) is composed of a reactor, two independent vacuum systems, a mass spectrometer, and a mass-flow calorimeter. The reactor is depicted in Figure 3 and is composed of several components:

- A reactor core (RC), made out of a Swagelok 1/4" 25 cm long pipe, closed at one end by a vacuum tight TIG welding. The sample is 1 g of hydrated Ti powder (SAES Getters Group) and is placed inside the reactor core. In a second series of experiments a 1/4" custom-made alumina tube, closed at one end, has been used in place of the Swagelok tube to avoid steel melting at high temperature.
- Four N-type, Nicrosil-armored thermocouples of a thickness of 1.5 mm (TC1, TC2, TC3, and TC4).
- A flange equipped with 5 vacuum tight feed-through (F1).
- A hollow cylindrical heater (H1), inner diameter 10 mm, 15 cm length, made of 80 coils of Niconel wire, 1 mm diameter, and able to deliver up to 1 kW of thermal power. The RC can reach up to 1200°C. H1 surrounds RC so that the middle point of H1 is at the same height of the bottom of RC.
- An external vacuum chamber (C1), 56 mm diameter and 250 mm long, surrounding the reactor core and the heater, and filled with an insulating wool. C1 is sealed at its top by flange F1 and evacuated by the pump S1 (Figure 4). The temperature of the side walls and of the flange remains below 50°C even when RC reaches 1200°C thanks to the cooling system. Figure 5 shows the power–temperature calibration curve.
- An external plexiglass cylinder (C2) surrounding the external vacuum chamber where a water flow is allowed to circulate so that the reactor is cooled.
- Two PT100 water-resistant sensors (PTin, PTout) used for measuring the temperature of the inlet and outlet water.
- A water flow meter (FM), used for measuring the flow rate of the cooling water.
- A DC power supply, PS1, programmable from 0 to 500 V, 1 kW to feed H1.
- An amperometric resistance R1 of 1 Ω.
- Two Agilent multimeters, MM1 and MM2, model 2000, equipped with multiplexer cards.
- An RGA MS1, model Pfeiffer Prisma 80, equipped with TalkStar software, Version 1.40.

- A rotative+turbo pump connected directly downstream the MS1, capable of reaching a vacuum $\sim 10^{-7}$ mbar in the detection volume of MS1.
- A micro-needle, K1, that, together with valve G2, allows for a pressure drop from atmospheric down to the range of 10^{-7} mbar in the section directly connected to T1 and MS1.
- A PC running the LabView program that acquires all the digital data coming from MM1 and MM2 and stores them into a file for offline analysis.

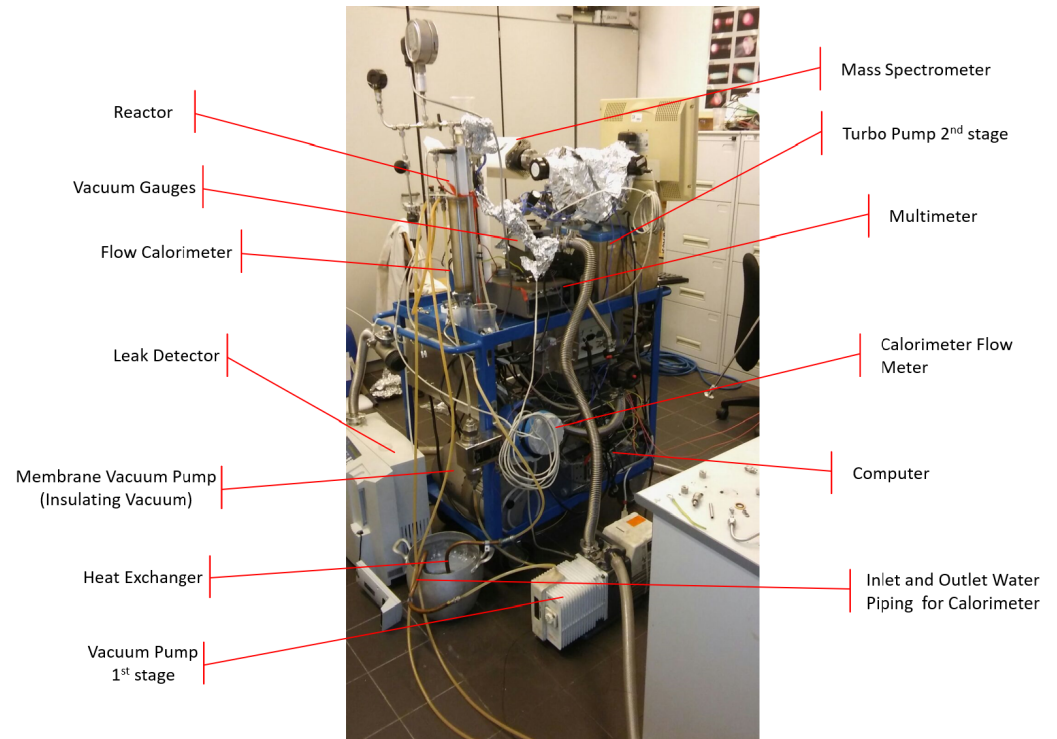


Figure 2. Global view of the complete experimental apparatus (zeolite filter not present in this configuration).

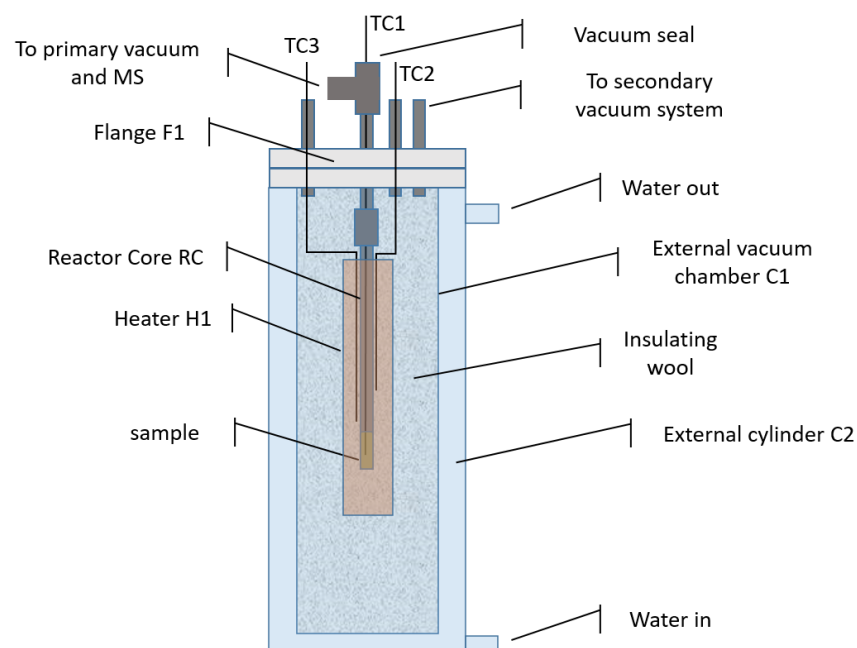


Figure 3. Schematics (not to scale) of the reactor.

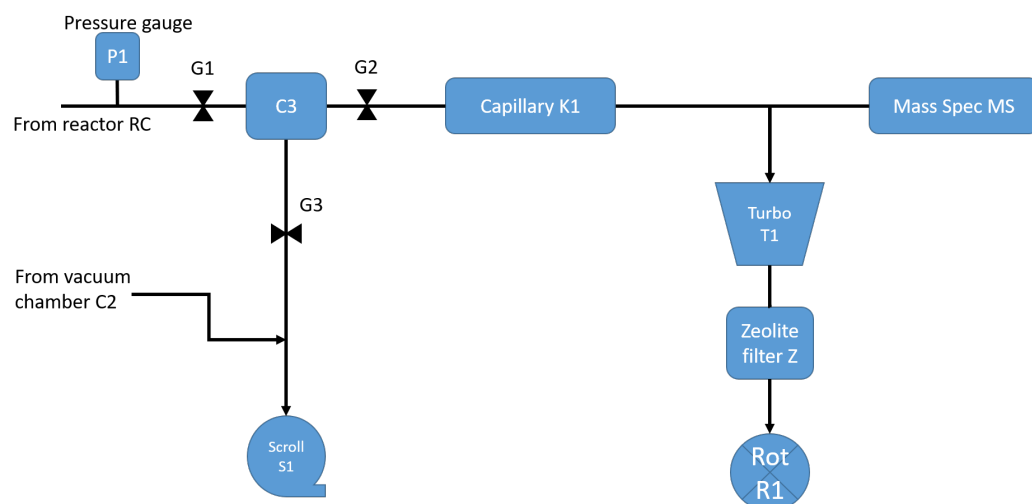


Figure 4. Schematics of the vacuum manifold.

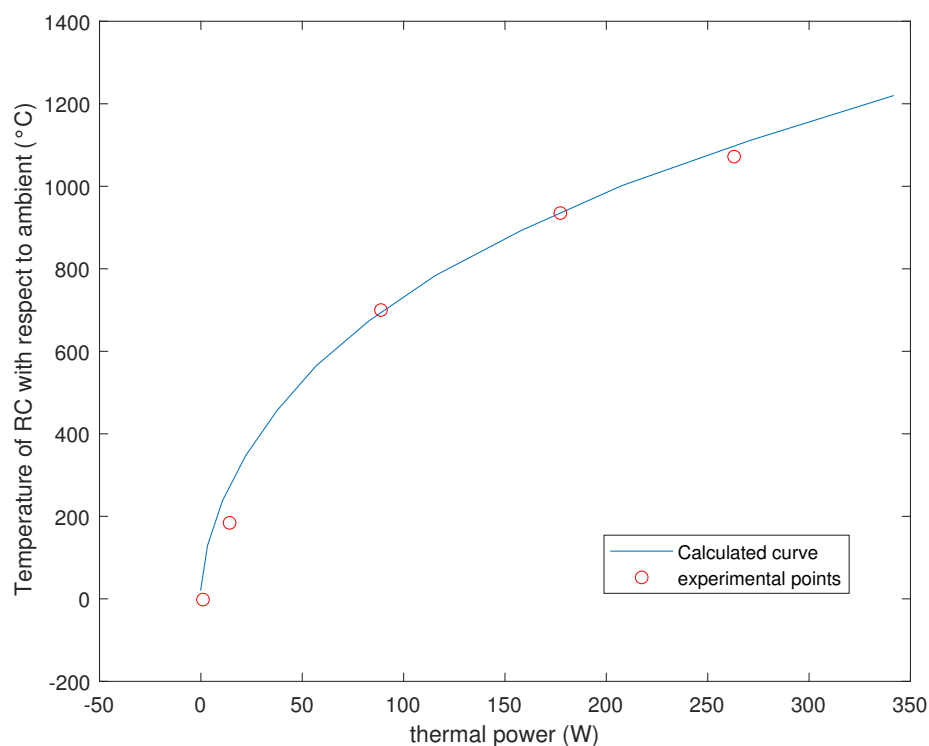


Figure 5. Calculated and measured temperature of RC at various heating powers. Thermal insulation is very good ($\sim 14\text{C/W}$ at room temperature).

The thermocouple TC1 is positioned inside RC so that the tip is 1 cm from the bottom of RC and about 2 cm below the top of the TiH_x powder.

RC is connected to F1 through a vacuum fitting in its turn connected to the primary vacuum system (see Figure 4). This flange seals a secondary vacuum chamber encompassing the reactor core. This arrangement establishes two distinct vacuum systems. The first, connected to RC (primary), is linked to the MS system, while the second (secondary) is connected to C1. The secondary system serves the dual purpose of enhancing thermal insulation for RC against the external environment (see Figure 5) and evacuating the intermediate chamber C3 upstream of the needle valve. A scroll, oil-free pump, S1 (Agilent SH-110 dry scroll vacuum pump, with a minimum pressure of $7 \cdot 10^{-2}$ mbar), is employed to pump the secondary vacuum system.

All tubing from RC to C3 consists of 1/4" Swagelok vacuum tubes. The remaining tubes are standard KF32 vacuum tubes equipped with a heating wire for degassing during the pump-down phase. A pressure gauge, P1, is situated on the vacuum manifold between RC and G1, measuring the pressure of gases released by the sample. Voltage measurements, V1 and V2, are recorded at the ends of H1 and R1, respectively, to precisely quantify the power supplied to H1.

Within the high-vacuum section of the primary vacuum system, near the MS, a Pirani vacuum gauge, P2, is installed to monitor vacuum quality during MS measurements. TC1, TC2, TC3, TC4, P1, V1, and V2 are connected to MM1 and MM2, which, in turn, are linked to a PC via the GPIB communication protocol. The experiment is orchestrated by a LabView program tailored for this purpose, capable of recording the complete set of raw data for subsequent offline analysis. The data acquisition is conducted at intervals of approximately 4 s.

The MS measurement is interfaced via RS-232 to the PC, and real-time acquisition data is stored in a text data file. H1 heats the RC, with its connections passing through the upper flange. In the interstice between RC and H1, TC2 and TC3 are positioned at different heights, with their connections also passing through the vacuum fittings present on F1. Finally, TC4 measures ambient temperature.

The gases released by the heated Ti powder are collected in C3 and can be sampled by MS1 thanks to the adjustable micro-needle valve (G2+K1 in Figure 4) that allows for a pressure drop from atmospheric down to the range of 10^{-7} mbar.

3.2. Experiment

The aim of the experiment was to subject TiH_x powders to thermal cycles in the range of 20–1100 °C in order to induce rapid hydrogen degassing fluxes. During this process, the RGA monitored the isotopic composition of the gases in the vacuum chamber. The expected result was that, following the intense hydrogen degassing, the coherent vibrational states in the metal would be sufficiently excited to produce ULM neutrons. The excess neutrons were then identified by detecting an increase in the isotopic abundance of deuterium.

The experiment commenced with the TiH_x powder at room temperature, while the primary vacuum system was maintained at approximately 90 °C and evacuated for three days with all G1, G2, and G3 valves open. The water contamination level was monitored using mass spectrometry (MS). Once the partial pressure of water reached around $5 \cdot 10^{-7}$ mbar, the vacuum system was returned to ambient temperature, and the experiment began. Valves G1, G2, and G3 were closed, and the power supplied to the heater was gradually increased, causing the temperature of the resistance coil (RC) to rise. Upon reaching a temperature of approximately 200 °C, the hydrogen loaded into the TiH_x sample began to degas.

During the degassing process, valves G1 and G2 were operated to maintain the pressure inside the MS manifold within the operating range of the MS. The pressure reading P2 was kept in the range of 10^{-7} – 10^{-5} mbar, and peaks at $m/z = 1, 2, 3, 4, 18, 19, 20,$ and 21 were continuously monitored.

The parameters of the experiment were recorded every 4 s and stored for later analysis. The temperature of the sample was gradually increased, as displayed in Figure 6, up to a maximum of approximately 1100 °C. At this point, the reactor core (RC in Figure 3) underwent a meltdown, contaminating the analyzed gas with air from chamber C1, which concluded the experiment.

The choice of a wide temperature range (20–1000 °C) was made to ensure that the entire degassing process of TiH_2 was covered. Titanium hydride undergoes significant degassing over a broad temperature range, with hydrogen release beginning around 400 °C and continuing through 700 °C, as described in the literature. This range was also chosen to perform calorimetry over the full temperature spectrum to ensure that any potential anomalous heat generation could be detected. As shown in Figure 6, no measurable

excess heat was observed throughout the experimental range. The experiment aimed to investigate any calorimetric anomalies during the degasification process, and the wide temperature interval was necessary to capture all relevant phase transitions and potential thermal effects.

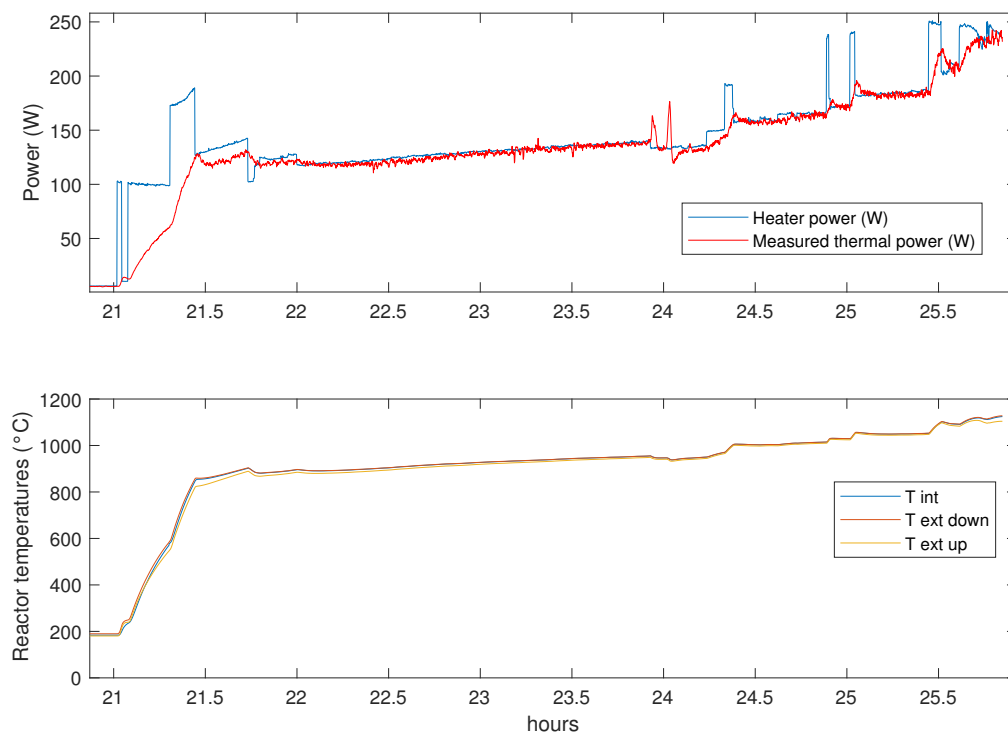


Figure 6. Time evolution of heating power (upper panel) and temperatures of the cell (lower panel).

The experiment was conducted seven times using both the gas outgassed from the cell and a reference H_2 tank, with careful attention to maintaining consistent experimental conditions throughout all trials. The results consistently reflected those obtained from both the active cell and the reference, highlighting the differences between the outcomes with the active powder and the reference gas, which will be detailed in the following section.

4. Results

The experimental results using mass spectrometry suggest the production of deuterium in Ti powders with a high loading ($x \simeq 2$) of natural hydrogen. The gas released from the powders is injected into the RGA to analyze the relative abundance of gas species present in the chamber during the thermal cycles. The detection of deuterium excess is obtained with a number of independent methods, all relying on low-resolution mass spectrometry analyses. The methods are as follows:

- Monitoring of the peak intensity at $m/z = 3$ compared to the peak intensity at $m/z = 2$;
- Monitoring of the peak intensity at $m/z = 4$ compared to the peak intensity at $m/z = 2$;
- Monitoring of the peak intensity at $m/z = 19$ and $m/z = 21$ compared to the peak intensity at $m/z = 18$.

These methods will be described in detail in the following.

4.1. Signal Intensity of HD

Figure 7 illustrates the typical mass spectra obtained before and after melting of the reactor at approximately 1100 °C. Figure 8 depicts the intensity ratio between $m/z = 3$ (HD) and $m/z = 2$ (H_2) species for the gas produced in the reaction and for the gas from an H_2 bottle used as a reference. The labels “exp1” and “exp2” correspond to experiments conducted with the active cell, while the “ref1” and “ref2” labels are relevant to the tests

using the gas from the H_2 reference tank. All measurements are conducted under identical conditions. A noticeable discrepancy of η_3 is evident when the powder is present, compared to the value measured using an H_2 tank. However, anomalous behavior for the case of atomic hydrogen (η_1) is not observed in this context. A significant increase in the relative abundance of the $\eta_3 = (m/z = 3)/(m/z = 2)$ signal is observed compared to the same quantity η_3^{ref} measured in the reference gas in identical conditions. Figure 8 shows that the measurements have been performed several times, always giving consistent results.

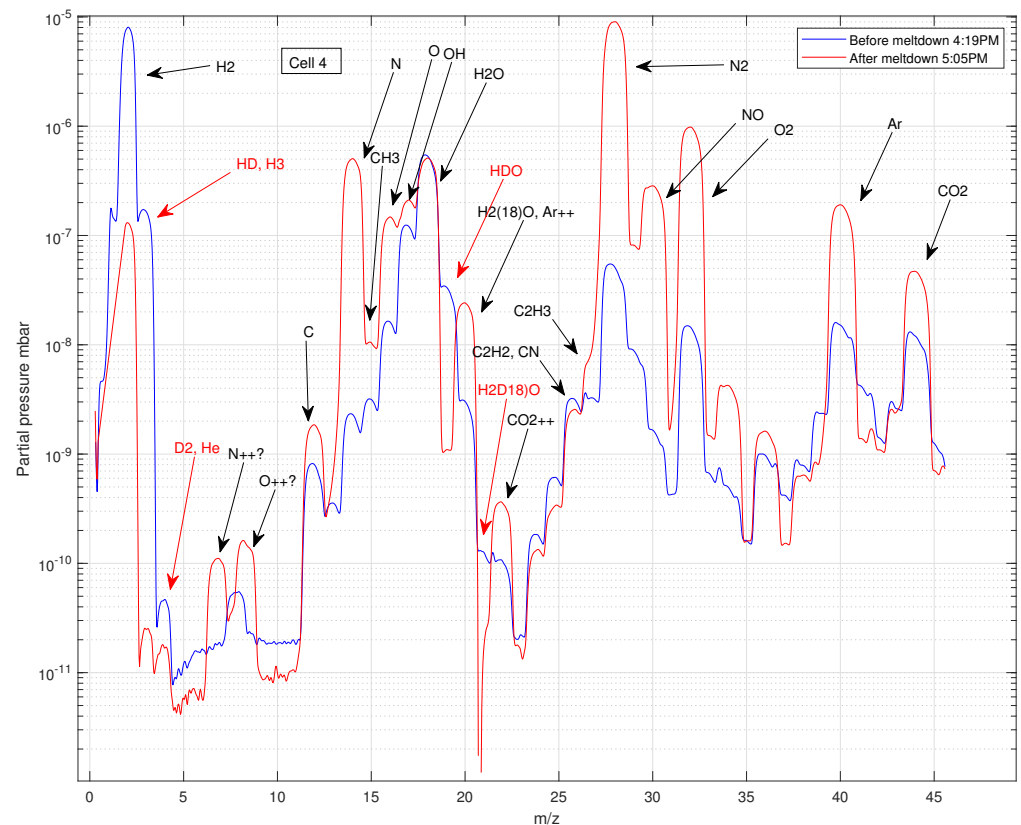


Figure 7. Mass spectrum of the outgassed elements from the TiH_x powder before and after melting of the cell. After melting, clear air contamination is present. In red are highlighted the peaks attributed to the presence of excess deuterium.

Figure 9 illustrates the variation in the peak ratios η_3 and η_4 for the species at $m/z = 3$ and $m/z = 4$ measured during the experiment, along with the corresponding values η_3^{ref} and η_4^{ref} obtained for the reference H_2 bottle. The evident excess signal observed during the experiment compared to the reference signal is noteworthy. Furthermore, it is notable that the variations in η_3 and η_4 with pressure align with the anticipated behavior. Specifically, the partial pressure variation for HD is expected to demonstrate a linear relationship with the pressure of H_2 , while the partial pressure of D_2 is expected to vary quadratically. Consequently, η_3 is anticipated to remain constant with changes in the pressure of H_2 , while η_4 is expected to be directly proportional to the pressure of H_2 . The observation confirms such an outcome within the experimental error.

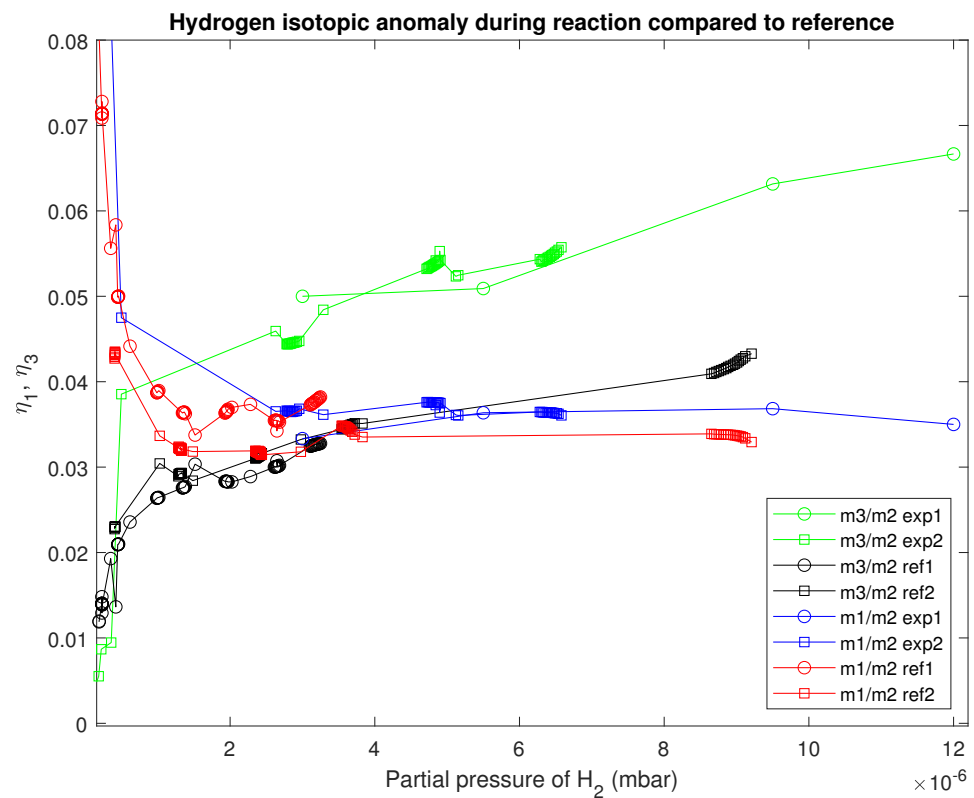


Figure 8. Ratio of MS intensities $\eta_1 = P_1/P_2$ and $\eta_3 = P_3/P_2$ at $m/z = 1$ and $m/z = 3$ compared to the intensity at $m/z = 2$ in four distinct experiments: two involving the TiH_x powder (green and blue curves) and the other two using hydrogen from a tank (red and black curves).

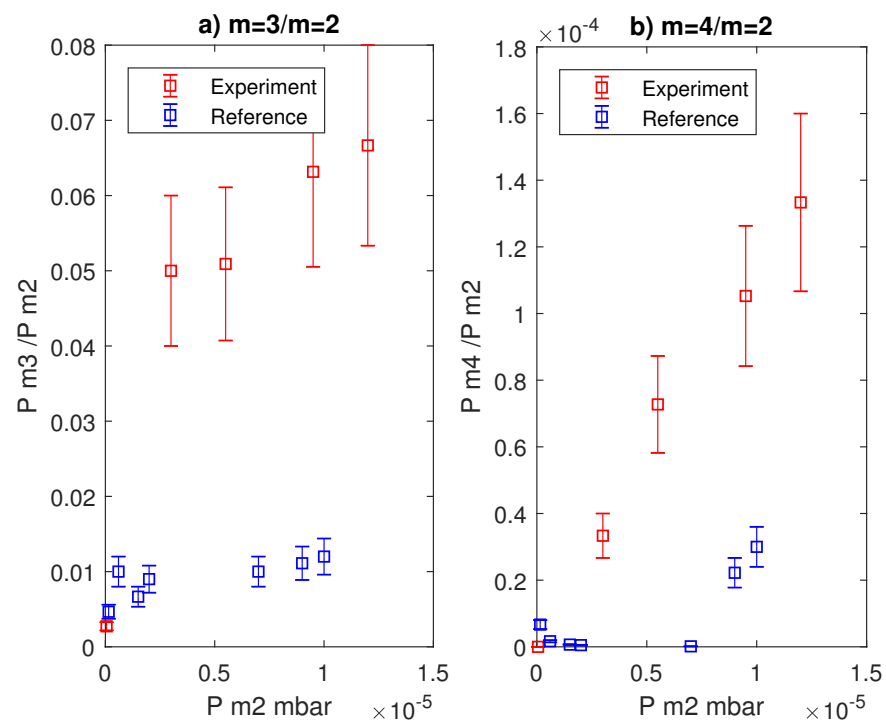


Figure 9. Ratio of the intensities for $m/z = 3$ and $m/z = 4$ to $m/z = 2$ in the case of the experiment using the TiH_x powder and using the hydrogen from a tank. The different value of the ratio for $m/z = 3$ when the powder is present from the value measured using a H_2 tank is clear.

4.2. The H_3^+ Problem

In Refs. [29,30], the investigation reveals that the measurement of HD abundance in mass spectroscopy requires correction due to the formation of H_3^+ in the ionized plasma within the mass spectrometer. This formation is a result of the following reaction:



Given that H_3^+ is not distinguishable from HD^+ by typical isotope ratio mass spectrometers, a correction becomes necessary. The concentration of H_2^+ is directly proportional to the partial pressure of H_2 ; consequently, the generation of H_3^+ is proportional to the square of the partial pressure of H_2 . To correct the height of the $m/z = 3$ peak, the following formula is applied:

$$P_{HD} = P_3 - KP_2^2 \quad (5)$$

Here, P_{HD} represents the partial pressure in mbar of the HD^+ ion, while P_2 and P_3 are the intensities measured in mbar at $m/z = 2$ and $m/z = 3$, respectively. The correction constant K has been determined to be approximately $5000\text{--}30,000 \text{ mbar}^{-1}$ (see Ref. [30]), assuming a sensitivity of 1 mA/mbar.

Equation (5) indicates that, when $P_2 \sim 8 \cdot 10^{-6}$ mbar, the correction due to H_3 is in the order of $P_{H_3} \sim 3 \cdot 10^{-7} - 2 \cdot 10^{-6}$ mbar. This value can potentially overshadow the contribution of the HD signal. In the absence of a high-resolution mass spectrometer, an alternative method for detecting HD concentration involves monitoring the intensity ratio $\eta_3 = P_3/P_2$ as a function of the H_2 pressure, proportional to P_2 . Using Equation (5), we can express η_3 as follows:

$$\eta_3 = \frac{P_{HD}}{P_2} + KP_2 \quad (6)$$

This allows the extraction of the interesting quantity $\eta_3^0 = \lim_{P_2 \rightarrow 0} \frac{P_3}{P_2}$, which represents the real estimate of the abundance ratio of deuterium, by linearly fitting the values of η_3 measured at various H_2 pressures.

Continuing along the same line of thought, we can theoretically formulate the relationship between the pressure of H_2 and the peak ratio $\eta_4 = P_4/P_2$, which represents the ratio of intensities at $m/z = 4$ and $m/z = 2$. Given the minimal signal contribution from 4He , we attribute the observed value to the presence of D_2 . The concentration of D_2 is expected to vary in direct proportion to the square of the pressure of H_2 (refer to Table 1) being $[D_2] \propto [D_1]^2 \propto [H_2]^2$, in the absence of any linear contribution. Consequently, if η_4 is contingent upon the concentration of D_2 , an anticipated linear variation with P_2 emerges.

Table 1. Most relevant reactions involving hydrogen, deuterium, and oxygen.

Reactants		Products	Reaction Rate
$H_1 + H_1$	\longleftrightarrow	H_2	$[H_2] = k_1[H_1]^2$
$D_1 + D_1$	\longleftrightarrow	D_2	$[D_2] = k_1[D_1]^2$
$H_2 + H_1$	\longleftrightarrow	H_3	$[H_3] = k_2[H_2][H_1]$
$H_2 + H_2$	\longleftrightarrow	$H_3 + H_1$	$[H_3][H_1] = k_3[H_2]^2$
$HD + DH$	\longleftrightarrow	$D_2 + H_2$	$[H_2][D_2] = k_4[HD]^2$
HDO	\longleftrightarrow	$D + OH$	$[D_1][OH] = k_5[HDO]$
HDO	\longleftrightarrow	$HD + O$	$[HD][O] = k_6[HDO]$
H_2O	\longleftrightarrow	$H + OH$	$[H_1][OH] = k_7[H_2O]$

Figure 8 shows the variation in η_3 and η_4 together with the ratios with the $m/z = 1$ peak for the experiment and reference case.

Figure 9 shows the variation in η_3 and η_4 with varying H_2 pressures. Both quantities are shown in the case of gas released during the experiment and of gas originated from a H_2 tank, taken as the reference for the natural abundance and measured in completely identical conditions. The variation in η_3 is linear within the experimental errors and displays an

intercept different from zero, as expected from theory. The variation in η_4 is also linear within the experimental errors and displays an intercept compatible with zero, as expected from theory. The results of the linear fits are shown in Table 2. The value of η_3^0 represents the expected relative abundance of deuterium compared to normal hydrogen, 280 times larger than the natural value 160 ppm.

Table 2. Linear fit of the data shown in Figure 9 with 95% confidence intervals.

Experiment	η_3^0 with Interval at 95% Confidence Level	η_4^0 with Interval at 95% Confidence Level	Adjusted R-Square 3	Adjusted R-Square 4
Experiment 1	0.045 (0.037, 0.053)	$1.04 \cdot 10^{-5}$ ($-2.6 \cdot 10^{-5}$, $4.7 \cdot 10^{-5}$)	0.95	0.98
Reference 1	0.008 (0.006, 0.011)	$-4.75 \cdot 10^{-6}$ ($-2.1 \cdot 10^{-5}$, $1.2 \cdot 10^{-5}$)	0.49	0.84

The comparison with the reference gas shows an excess in the concentration of HD and D_2 well above the experimental errors, thus confirming the hypothesis of deuterium production during the experiment.

4.3. Observation of Deuterated Water

Another independent indication of the presence of an excess of deuterium compared to the natural abundance can be detected by measuring the relative intensity of the peaks associated with the water molecule.

The possible isotopic combinations for the water molecule are listed in Table 3, together with their natural relative intensities.

Table 3. Natural abundance of mass peaks of the water molecule (derived from [31–33]).

m/z	Relative Intensity	Isotopic Combinations
18.0106	100	$H_2^{16}O$
19.0148	0.0401	$H_2^{17}O$
19.0169	0.032	$HD^{16}O$
20.0148	0.2001	$H_2^{18}O$
20.0211	$1.284 \cdot 10^{-5}$	$HD^{17}O$
20.0231	$2.56 \cdot 10^{-6}$	$D_2^{16}O$
21.0211	$6.42 \cdot 10^{-5}$	$HD^{18}O$
21.0273	$1.03 \cdot 10^{-9}$	$D_2^{17}O$
22.0274	$5.13 \cdot 10^{-9}$	$D_2^{18}O$

In Table 4 are shown the measured intensities during the experiment and after the meltdown of the reactor with air contamination. The peak of ^{40}Ar increases after meltdown due to the air contamination, allowing for a determination of the intensity ratio r_{Ar} between $^{40}Ar^{++}$ and $^{40}Ar^+$. We find $r_{Ar} = 0.1268$ that can be used to subtract the unknown contribution of $^{40}Ar^{++}$ from the intensity of the peak at $m/z = 20$ measured during the experiment. The procedure is facilitated by the notable increase in the $^{40}Ar^+$ signal post-meltdown, leading to a substantial predominance of $^{40}Ar^{++}$ over the $H_2^{18}O$ signal.

After the correction, we compute the ratios of the measured intensities with the corresponding natural values as shown in Table 5 that shows a very large increase in deuterium abundance compared to the natural abundance. The ratios at $m/z = 19$ and $m/z = 21$ are both notably higher than 1, contrasting with the corresponding values measured after the reactor meltdown. This discrepancy suggests an excess of deuterium during the reaction compared to the natural abundance. Despite the anticipation that their values should be equal, the observed difference remains unexplained. It is likely that unidentified contributions are introducing additional signals, adding complexity to the interpretation of the sought-after signal.

Figure 10 presents the temporal evolution of $\eta_{19} = P(m/z = 19)/P(m/z = 18)$ throughout the experiment, shown by the red line, spanning from the start of the heating ramp until the cell melts at temperatures between 1100 and 1200 °C, coinciding with air contamination. A marked increase in η_{19} appears as the degassing of the TiH_x powder begins. To sustain optimal RGA functionality, the pressure is regulated by adjusting the needle valve, ensuring that the H_2 partial pressure remains within an acceptable range. Also included in Figure 10 is η_{19}^{ref} , representing the analogous ratio measured from gas released by the reference H_2 bottle, which shows no significant fluctuations in this case.

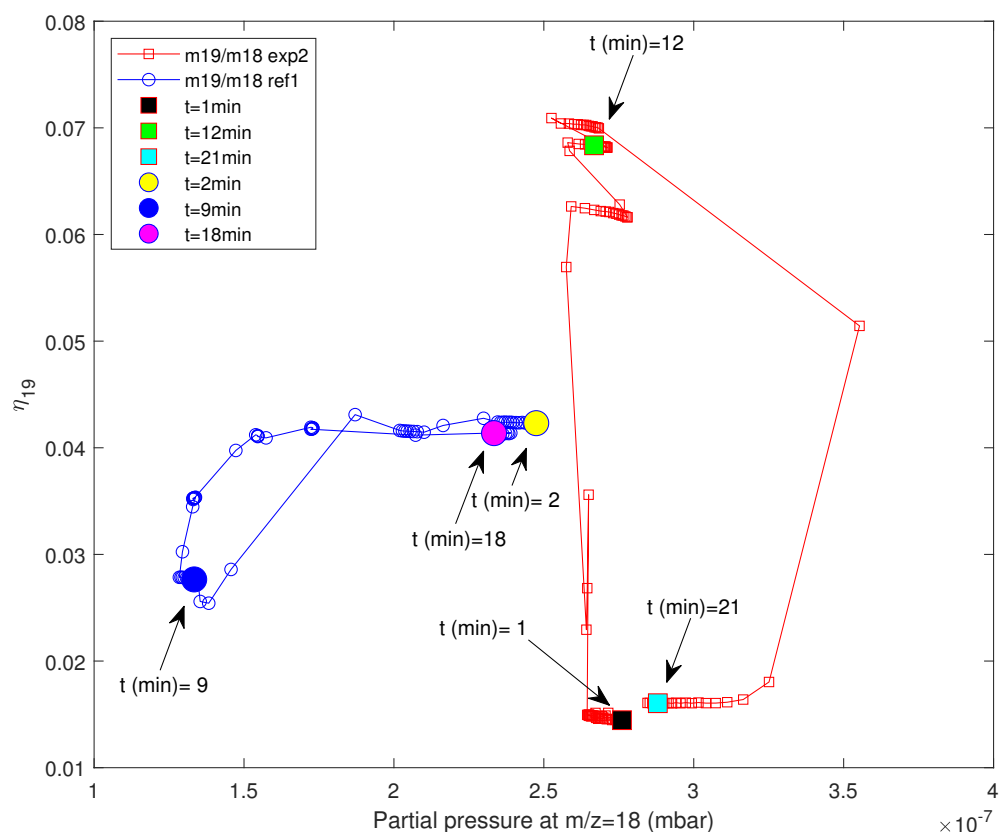


Figure 10. The temporal evolution of η_{19} is depicted during the experiment involving an active cell (represented by the red line) and with a reference gas obtained from an H_2 bottle (indicated by the blue line).

Table 4. Observed peak intensities in the range 18–22 m/z during the experiment and after reactor meltdown with air contamination, along with the possible attribution to chemical species (see Figure 7).

m/z	Partial Pressure (mbar) During the Experiment	Partial Pressure (mbar) After Meltdown	Identification
18	$5.5 \cdot 10^{-7}$	$5.1 \cdot 10^{-7}$	$H_2^{16}O$
19	$3.5 \cdot 10^{-8}$	$1.1 \cdot 10^{-9}$	$HD^{16}O, H_2^{17}O$
20	$3.1 \cdot 10^{-9}$	$2.4 \cdot 10^{-8}$	$H_2^{18}O, HD^{17}O, D_2^{16}O, {}^{20}Ne, {}^{40}Ar^{++}$
21	$1.3 \cdot 10^{-10}$	0	$HD^{18}O, D_2^{17}O, {}^{21}Ne$
22	$1.1 \cdot 10^{-10}$	$3.8 \cdot 10^{-10}$	$D_2^{18}O, {}^{22}Ne, CO_2^{++}$
40	$1.6 \cdot 10^{-8}$	$1.9 \cdot 10^{-7}$	${}^{40}Ar$

Table 5. Ratio of the measured intensities with the natural intensities. An isotopic excess for deuterium is detected. The increased signal observed at $m/z = 20$ after the meltdown is attributed to $^{40}\text{Ar}^{++}$ and ^{20}Ne , which were practically absent during the experiment but significantly increased after air contamination due to their presence in the atmosphere.

m/z	Before Meltdown	After Meltdown	Species
18	1.00	1.00	H_2^{16}O
19	87.7	2.98	HD^{16}O
20	0.998	23.5	H_2^{18}O
21	233	0	HD^{18}O

The η_{19} value rises rapidly with increasing cell temperature, then returns to its initial level after the cell meltdown. This behavior suggests an increase in deuterium nucleus concentration within the gases released by the TiH_x sample. These gases react with OH^- radicals to produce HDO , with a mass peak at $m/z = 19$. No notable variation in the ratio is observed when reference H_2 is introduced from the H_2 tank (blue line). The likelihood that the peak at $m = 19$ amu arises from H_3O is considered highly improbable [33], making an actual increase in D concentration the most probable cause of this rise.

To summarize this section, we have shown in three independent ways a significant increase in deuterium concentration well above the natural background after the intense degassing of TiH_x powders subjected to rapid thermal excitations.

5. Discussion

This study marks a significant advancement in developing a unified scientific framework to comprehend nuclear phenomena in deuterated or hydrated metals, integrating both experimental and theoretical perspectives.

The theoretical process under investigation in this work does not exhaustively account for all mechanisms that could lead to nuclear processes at low energy. Rather, it represents one potential pathway for initiating nuclear transmutations. Notably, an alternative process that could induce nuclear reactions at low temperatures is the fusion of deuterium nuclei within palladium, as outlined in [34]. Further theoretical contributions have been made by Hagelstein et al. [35]; yet, a unifying aspect across these diverse mechanisms is the quantum coherence that underpins such processes [36].

A critical aspect of these processes, particularly in scenarios involving a limited number of participating particles, is the challenge of dissipating the substantial energy released (in the order of several MeV) as thermal heat. In contrast, only processes involving a large ensemble of particles can effectively mitigate the emission of highly energetic particles, a stark difference from traditional nuclear reactions observed in conventional nuclear reactors. Energetic radiation in low-energy nuclear reactions becomes detectable only under specific non-equilibrium conditions, as evidenced by the work of G. Carpinteri and colleagues [25], who observed reproducible bursts of neutrons during controlled rock fracturing experiments.

This study integrates theoretical insights with experimental findings, offering a comprehensive analysis of deuterium production from titanium hydride powders subjected to thermal cycling. The theoretical framework suggests the possibility of neutron generation via electron capture within metal samples heavily loaded with hydrogen, a process enabled by the coherence properties of the quantum plasma formed by dissolved protons in the metal.

The central premise of this study, alongside the work referenced in [18], posits that a deeper understanding of low-energy nuclear reactions (LENRs) hinges on the stimulation of coherent configurations. These configurations facilitate either weak or strong interactions that would be otherwise unattainable in few-body dynamics due to the insufficient energy available. In the specific case examined, the existence of ultra-low momentum (ULM)

neutrons triggers neutron capture processes, leading to the production of deuterium, tritium, and various titanium isotopes.

The experimental results reveal an anomaly in deuterium–hydrogen (*HD*) ratios, emphasizing the potential production of deuterium in Ti powders. Mass spectrometry analyses show an increase in deuterium abundance, with three independent methods confirming the deuterium excess. The isotopic anomaly is further supported by the observation of deuterated water and the analysis of water molecule peaks.

One critique that could be raised against the obtained result is that the measured excess concentration of deuterium is not due to the actual production of deuterium nuclei in the metal matrix, but rather to the isotopic effect in titanium desorption rates, which favors the concentration of deuterium in the outgassed gas that reaches the mass spectrometer. However, this criticism is refuted by previous experimental observations, which demonstrate that titanium shows no diffusion and degassing differences among the various isotopes of hydrogen, deuterium, and tritium [37], or, in some cases, the diffusion is slower for deuterium than for hydrogen [38].

The question may arise whether the obtained results can be influenced by the chemical activity of hydrogen with the reactor core at high temperatures. However, no matter how complex the reactions involving hydrogen may be, the variation in peak heights will be the same for hydrogen and deuterium. Consequently, the ratio of the peak heights corresponding to hydrogen and deuterium cannot depend on such chemical reactions. Therefore, a change in temperature cannot alter this ratio. Any observed variation in this ratio should thus be attributed to actual changes in the concentration of deuterium relative to that of hydrogen.

It is also crucial to note that the entire vacuum system, RGA, reactor, or any other part of the experimental equipment has never been directly exposed to a source of deuterium that could explain the obtained findings as a result of mere deuterium contamination.

6. Conclusions

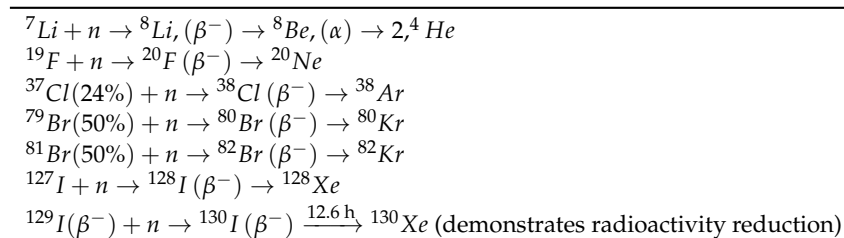
This work demonstrates, for the first time to our knowledge, the production of deuterium through the thermal excitation of titanium powders loaded with hydrogen. This experimental result was motivated by theoretical studies predicting the generation of neutrons within the metal under appropriate stimulation. The presence of neutrons implies deuterium production, creating a coherent link between the experimental results and theoretical predictions that mutually reinforce each other. The main conclusions of our study are as follows:

- **Experimental Evidence:** Mass spectrometry analyses revealed an unexpected increase in the deuterium-to-hydrogen ratio in the degassing gases from the titanium hydride samples, with the deuterium concentration rising up to 280 times its natural abundance. These results were confirmed through three independent measurement methods.
- **Novelty of the Work:** The primary innovation of this research lies in confirming the coherence-driven electron capture mechanism that leads to neutron production and subsequent deuterium synthesis in metal hydrides. This previously unobserved neutron generation opens new avenues in understanding low-energy nuclear reactions (LENRs) within solid-state physics.
- **Theoretical Consistency:** The observed experimental results are in agreement with a theoretical framework based on electroweak interaction theories, specifically employing gauge symmetry to predict ultra-low momentum neutron generation through coherent vibrational excitations.
- **Technological and Scientific Implications:** This work presents a pathway for applications in isotope production, nuclear waste remediation, or advanced energy devices utilizing solid-state nuclear reactions. The potential for neutron generation via this method could significantly impact energy and material sciences.
- **Future Directions:** Further research is planned to expand our understanding of the conditions enabling these coherent states that facilitate nuclear transformations. Pro-

posed experiments will investigate similar processes in alternative metal matrices and explore practical applications with a focus on sustainable energy and environmental solutions.

In line with these findings, further experiments are proposed to validate the applicability of the theory described in [18] to other nuclei beyond deuterium. To test this hypothesis and assess the method's potential for practical applications, such as isotope production and nuclear waste remediation, the reactions listed in Table 6 have been selected. These reactions aim to produce noble gases, which are ideal for detection due to their chemical inertness and minimal interaction with the system materials, thus ensuring reliable analysis. The specific noble gas of interest depends on the isotopes which are supposed to be present in the initial samples. Notably, transmuting the long-lived isotope ^{129}I into stable ^{130}Xe could demonstrate the ability to inertize radioactive substances, further underlining the method's practical relevance for waste management.

Table 6. Possible reactions involving neutrons whose final products are noble gases.



In conclusion, this study integrates theoretical insight with experimental validation, marking a significant step forward in the scientific understanding of nuclear processes in metal hydrides. By bridging theory with experimental findings, it establishes a foundation for future work in LENR and solid-state nuclear technology, with applications in isotope production, environmental sustainability, and nuclear waste management.

Author Contributions: L.G. conceived and conducted the experiments and analyzed the results, and L.G. and G.M. developed the theoretical interpretation. Conceptualization, L.G. and G.M.; methodology, L.G.; software, L.G.; formal analysis, L.G. and G.M.; data curation, L.G.; writing—original draft preparation, L.G.; writing—review and editing, L.G. and G.M. All authors have read and agreed to the published version of the manuscript.

Funding: This research received no external funding.

Data Availability Statement: The original contributions presented in the study are included in the article; further inquiries can be directed to the corresponding author.

Acknowledgments: We extend our gratitude to Alessandro Mietner for ensuring the proper functioning of all vacuum systems and for constructing the necessary mechanical components for the experiment. We are also grateful to Claudia Riccardi for her valuable support in this research. Finally, we thank Emilia Bossi for her support and continuous encouragement.

Conflicts of Interest: The authors declare no conflicts of interest.

References

- De Ninno, A.; Frattolillo, A.; Lollobattista, G.; Martinis, L.; Martone, M.; Mori, L.; Podda, S.; Scaramuzzi, F. Evidence of emission of neutrons from a titanium-deuterium system. *Europhys. Lett.* **1989**, *9*, 221. [\[CrossRef\]](#)
- Ohmori, T.; Enyo, M.; Mizuno, T.; Nodasaka, Y.; Minagawa, H. Transmutation in the Electrolysis of Light Water—Excess Energy and Iron Production in a Gold Electrode. *Fusion Technol.* **1997**, *31*, 210–218. [\[CrossRef\]](#)
- Ohmori, T.; Mizuno, T.; Nodasaka, Y.; Enyo, M. Transmutation in a Gold-Light Water Electrolysis System. *Fusion Technol.* **1998**, *33*, 367–382. [\[CrossRef\]](#)
- Iwamura, Y.; Sakano, M.; Itoh, T. Elemental analysis of Pd complexes: Effects of D2 gas permeation. *Jpn. J. Appl. Phys.* **2002**, *41*, 4642. [\[CrossRef\]](#)

5. Iwamura, Y.; Itoh, T.; Sakano, M.; Sakai, S.; Kuribayashi, S. Low energy nuclear transmutation in condensed matter induced by D₂ gas permeation through Pd complexes: Correlation between deuterium flux and nuclear products. In *Condensed Matter Nuclear Science*; World Scientific: Singapore, 2006; pp. 435–446.
6. Iwamura, Y.; Itoh, T.; Sakano, M.; Yamazaki, N.; Kuribayashi, S.; Terada, Y.; Ishikawa, T.; Kasagi, J. Observation of nuclear transmutation reactions induced by D₂ gas permeation through Pd complexes. In *Condensed Matter Nuclear Science*; World Scientific: Singapore, 2006; pp. 339–350.
7. Celani, F.; Spallone, A.; Righi, E.; Trenta, G.; Catena, C.; D'Agostaro, G.; Quercia, P.; Andreassi, V.; Marini, P.; Di Stefano, V.; et al. Innovative procedure for the, in situ, measurement of the resistive thermal coefficient of H(D)/Pd during electrolysis: Cross-comparison of new elements detected in the Th–Hg–Pd–D(H) electrolytic cells. In *Condensed Matter Nuclear Science*; World Scientific: Singapore, 2006; pp. 108–127.
8. Celani, F.; Spallone, A.; Righi, E.; Trenta, G.; Catena, C.; D'Agostaro, G.; Quercia, P.; Andreassi, V.; Marini, P.; di Stefano, V.; et al. Thermal and isotopic anomalies when Pd cathodes are electrolyzed in electrolytes containing Th–Hg salts dissolved at micromolar concentration in C₂H₅OD/D₂O mixtures. In *Condensed Matter Nuclear Science*; World Scientific: Singapore, 2006; pp. 379–397.
9. Srinivasan, M.; Miley, G.; Storms, E. Low energy nuclear reactions: Transmutations. In *Nuclear Energy Encyclopedia: Science, Technology and Applications*; Wiley: Hoboken, NJ, USA, 2011; pp. 503–540.
10. Iwamura, Y.; Itoh, T.; Yamazaki, N.; Kasagi, J.; Terada, Y.; Ishikawa, T.; Sekiba, D.; Yonemura, H.; Fukutani, K. Observation of low energy nuclear transmutation reactions induced by deuterium permeation through multilayer Pd and CaO thin film. *J. Condens. Matter Nucl. Sci.* **2011**, *4*, 132–144.
11. Iwamura, Y.; Itoh, T.; Tsuruga, S. Transmutation reactions induced by deuterium permeation through nano-structured palladium multilayer thin film. *Curr. Sci.* **2015**, *108*, 628.
12. Iwamura, Y.; Itoh, T.; Kasagi, J.; Kitamura, A.; Takahashi, A.; Takahashi, K.; Seto, R.; Hatano, T.; Hioki, T.; Motohiro, T.; et al. Anomalous heat effects induced by metal nano-composites and hydrogen gas. *J. Condens. Matter Nucl. Sci.* **2019**, *29*, 119–128.
13. Iwamura, Y.; Itoh, T.; Yamauchi, S.; Takahashi, T. Anomalous heat generation that cannot be explained by known chemical reactions produced by nano-structured multilayer metal composites and hydrogen gas. *Jpn. J. Appl. Phys.* **2024**, *63*, 037001. [[CrossRef](#)]
14. Hioki, T.; Takahashi, N.; Kosaka, S.; Nishi, T.; Azuma, H.; Hiibi, S.; Higuchi, Y.; Murase, A.; Motohiro, T. Inductively coupled plasma mass spectrometry study on the increase in the amount of Pr atoms for Cs-ion-implanted Pd/CaO multilayer complex with deuterium permeation. *Jpn. J. Appl. Phys.* **2013**, *52*, 107301. [[CrossRef](#)]
15. Metzler, F.; Hunt, C.; Messinger, J.; Galvanetto, N.; Hagelstein, P. Probing Neutrons and Purported Fission Daughter Products from Gas-Loaded, Laser-Irradiated Metal-Hydrogen Targets. 2023. Available online: <https://ssrn.com/abstract=4411160> (accessed on 11 November 2024).
16. Fomitchev-Zamilov, M. Observation of neutron emission during acoustic cavitation of deuterated titanium powder. *Sci. Rep.* **2024**, *14*, 2045–2322. [[CrossRef](#)]
17. Huang, B.J.; Pan, Y.H.; Wu, P.H.; Yeh, J.F.; Tso, M.L.; Liu, Y.H.; Wu, L.; Huang, C.K.; Chen, I.F.; Lin, C.H.; et al. Water can trigger nuclear reaction to produce energy and isotope gases. *Sci. Rep.* **2024**, *14*, 214. [[CrossRef](#)] [[PubMed](#)]
18. Gamberale, L. Neutron Production via Electron Capture by Coherent Protons. *arXiv* **2022**, arXiv:2209.06139.
19. Gamberale, L.; Modanese, G. Coherent Plasma in a Lattice. *Symmetry* **2023**, *15*, 454. [[CrossRef](#)]
20. Gamberale, L.; Modanese, G. Numerical simulations unveil superradiant coherence in a lattice of charged quantum oscillators. *Phys. Condens. Matter* **2023**, *671*, 1–8. [[CrossRef](#)]
21. Gamberale, L.; Modanese, G. Spectral Analysis of Proton Eigenfunctions in Crystalline Environments. *Quantum Rep.* **2024**, *6*, 172–183. [[CrossRef](#)]
22. Widom, A.; Larsen, L. Ultra low momentum neutron catalyzed nuclear reactions on metallic hydride surfaces. *Eur. Phys. J. C* **2006**, *46*, 107–111. [[CrossRef](#)]
23. Preparata, G. *QED Coherence in Matter*; World Scientific: Singapore, 1995; p. 104.
24. Mossin-Kotin, C.; Margolis, B.; Troubetzkoy, E.S. Calculations of Neutron Capture Cross Sections. *Phys. Rev.* **1959**, *116*, 937–938. [[CrossRef](#)]
25. Cardone, F.; Carpinteri, A.; Lacidogna, G. Piezonuclear neutrons from fracturing of inert solids. *Phys. Lett. A* **2009**, *373*, 4158–4163. [[CrossRef](#)]
26. Vysotskii, V.I.; Vysotskyy, M.V. Coherent correlated states and low-energy nuclear reactions in non stationary systems. *Eur. Phys. J. A* **2013**, *49*, 1–12. [[CrossRef](#)]
27. Bartalucci, S.; Vysotskii, V.; Vysotskyy, M. Correlated states and nuclear reactions: An experimental test with low energy beams. *Phys. Rev. Accel. Beams* **2019**, *22*, 054503. [[CrossRef](#)]
28. Ramkumar, K.; Kumar, H.; Jain, P. Low energy nuclear reactions through weak interactions. *Phys. Rev. C* **2024**, *110*, 044605. [[CrossRef](#)]
29. Sessions, A.L.; Burgoyne, T.W.; Hayes, J.M. Correction of H₃⁺ Contributions in Hydrogen Isotope Ratio Monitoring Mass Spectrometry. *Anal. Chem.* **2001**, *73*, 192–199. [[CrossRef](#)] [[PubMed](#)]
30. Sessions, A.L.; Burgoyne, T.W.; Hayes, J.M. Determination of the H₃ Factor in Hydrogen Isotope Ratio Monitoring Mass Spectrometry. *Anal. Chem.* **2001**, *73*, 200–207. [[CrossRef](#)] [[PubMed](#)]

31. Scientific Instrument Services (SIS). Isotope Distribution Calculator and Mass Spec Plotter. Available online: <https://www.sisweb.com/mstools/isotope.htm> (accessed on 11 November 2024).
32. NIST. Atomic Weights and Isotopic Compositions for All Elements. Available online: https://physics.nist.gov/cgi-bin/Compositions/stand_alone.pl?ele=&isotype=some (accessed on 11 November 2024).
33. NIST. Search for Species Data by Molecular Weight. Available online: <https://webbook.nist.gov/chemistry/mw-ser/> (accessed on 11 November 2024).
34. Bressani, T.; Del Giudice, E.; Preparata, G. First steps toward an understanding of «Cold» nuclear fusion. *Nuovo C* **1989**, *A*, 845–849. [CrossRef]
35. Metzler, F.; Hagelstein, P.; Lu, S. Observation of Non-Exponential Decay in X-Ray and γ Emission Lines from Co-57. *J. Condensed Matter Nucl. Sci.* **2018**, *27*, 46–96.
36. Fleischmann, M.; Pons, S.; Preparata, G. Possible theories of cold fusion. *Nuovo C* **1994**, *107*, 143–156. [CrossRef]
37. Wille, G.; Davis, J. Hydrogen in Titanium Alloys. Available online: <https://www.osti.gov/servlets/purl/6420120> (accessed on 11 November 2024).
38. Yamazaki, J.; Kobayashi, C.; Nishi, K.; Tanabe, K. Transport kinetics of protium and deuterium in titanium: Experiments and modeling. *Int. J. Hydrogen Energy* **2024**, *49*, 1483–1493. [CrossRef]

Disclaimer/Publisher’s Note: The statements, opinions and data contained in all publications are solely those of the individual author(s) and contributor(s) and not of MDPI and/or the editor(s). MDPI and/or the editor(s) disclaim responsibility for any injury to people or property resulting from any ideas, methods, instructions or products referred to in the content.